Monthly Notices
of the
ROYAL ASTRONOMICAL SOCIETY

MNRAS **457,** 1456–1467 (2016) doi:10.1093/mnras/stw074

On the nature of the most obscured C-rich AGB stars in the Magellanic Clouds

P. Ventura,[1]★ A. I. Karakas,[2,3] F. Dell'Agli,[1] D. A. García–Hernández,[4,5] M. L. Boyer[6,7] and M. Di Criscienzo[1]

[1]*INAF – Osservatorio Astronomico di Roma, Via Frascati 33, 00040, Monte Porzio Catone (RM), I-00077, Italy*
[2]*Research School of Astronomy and Astrophysics, the Australian National University, Canberra, ACT 2611, Australia*
[3]*Monash Centre for Astrophysics, School of Physics and Astronomy, Monash University, VIC 3800, Australia*
[4]*Instituto de Astrofísica de Canarias, E-38200 La Laguna, Tenerife, Spain*
[5]*Departamento de Astrofísica, Universidad de La Laguna (ULL), E-38206 La Laguna, Tenerife, Spain*
[6]*Observational Cosmology Lab, Code 665, NASA Goddard Space Flight Center, Greenbelt, MD 20771, USA*
[7]*CRESST and Department of Astronomy, University of Maryland, College Park, MD 20742, USA*

Accepted 2016 January 7. Received 2016 January 5; in original form 2015 November 18

ABSTRACT

The stars in the Magellanic Clouds with the largest degree of obscuration are used to probe the highly uncertain physics of stars in the asymptotic giant branch (AGB) phase of evolution. Carbon stars in particular provide key information on the amount of third dredge-up and mass-loss. We use two independent stellar evolution codes to test how a different treatment of the physics affects the evolution on the AGB. The output from the two codes is used to determine the rates of dust formation in the circumstellar envelope, where the method used to determine the dust is the same for each case. The stars with the largest degree of obscuration in the Large Magellanic Cloud (LMC) and Small Magellanic Cloud (SMC) are identified as the progeny of objects of initial mass 2.5–3 $M_\odot$ and ∼1.5 $M_\odot$, respectively. This difference in mass is motivated by the difference in the star formation histories of the two galaxies, and offers a simple explanation of the redder infrared colours of C-stars in the LMC compared to their counterparts in the SMC. The comparison with the *Spitzer* colours of C-rich AGB stars in the SMC shows that a minimum surface carbon mass fraction $X(C) \sim 5 \times 10^{-3}$ must have been reached by stars of initial mass around 1.5 $M_\odot$. Our results confirm the necessity of adopting low-temperature opacities in stellar evolutionary models of AGB stars. These opacities allow the stars to obtain mass-loss rates high enough ($\gtrsim 10^{-4}$ $M_\odot$ yr^{-1}) to produce the amount of dust needed to reproduce the *Spitzer* colours.

Key words: stars: abundances – stars: AGB and post-AGB – Magellanic Clouds.

1 INTRODUCTION

The recent years have witnessed a growing interest in the evolution of stars of low and intermediate mass ($M < 8\,M_\odot$), which evolve through the asymptotic giant branch (AGB) after the end of core helium burning. While this evolutionary phase only accounts for a very small percentage of the overall lifetime, it is extremely important because it is during the AGB when the richest nucleosynthesis occurs as well as the most intense mass-loss. This means that AGB stars are able to enrich their environment with gas chemically altered by internal nuclear processes and with the dust formed in their wind.

The unsolved problems of galaxy formation and chemical evolution at all redshifts require a full understanding of the topic of stellar evolution and nucleosynthesis of AGB stars. Particular areas where AGB stars have proven useful include inferring the masses of galaxies at high redshifts, owing to their large infrared (IR) luminosities (Maraston et al. 2006); chemical evolution of galaxies (Romano et al. 2010), owing to the ability of AGB stars to enrich their environment with stellar winds; because of the efficiency of the dust formation process in their winds, AGB stars play a crucial role in the formation and evolution of galaxies (Santini et al. 2014); recent studies suggested a relevant contribution from AGB stars to the dust content of high-redshift quasars (Valiante et al. 2011), contrary to earlier investigations, which stressed the dominant role of supernovae (Todini & Ferrara 2001; Nozawa et al. 2003; Maiolino et al. 2004); finally, AGB stars $\gtrsim 5\,M_\odot$ are one of the favoured

★ E-mail: paolo.ventura@oa-roma.inaf.it

© 2016 The Authors
Published by Oxford University Press on behalf of the Royal Astronomical Society

Downloaded from http://mnras.oxfordjournals.org/ at NASA Goddard Space Flight Ctr on May 24, 2016

polluters for providing the gas required to form second-generation stars in globular clusters (Ventura et al. 2001).

While theoretical models of AGB stars have seen significant progress over the last few years (e.g. Karakas & Lattanzio 2014), the results are still not completely reliable. This is primarily because we still do not understand how mass-loss or convection works in stars. The problem with convection manifests itself in two important ways in AGB stars. The first is through the efficiency of third dredge-up (TDU), which is the inward penetration of the convective envelope following each thermal pulse. The efficiency or depth of TDU depends on how convective borders are treated numerically (e.g. Frost & Lattanzio 1996). The second is through temperature gradients in convective regions, which cannot be calculated from first principles (Ventura & D'Antona 2005). Therefore, comparing theoretical AGB models with observations is crucial in order to substantially improve the predictive power of the stellar evolution models.

The Magellanic Clouds (MCs) are an ideal environment to test theoretical predictions, because they are relatively close [51 and 61 kpc, respectively, for the Large Magellanic Cloud (LMC) and Small Magellanic Cloud (SMC); Cioni et al. 2000a,b; Keller & Wood 2006] and the low reddening ($E(B-V) = 0.15$ and 0.04 mag, respectively, for the LMC and SMC; Westerlund 1997). Furthermore, the study of the MCs provides a wider range of possibilities in comparison with the Milky Way, because the interstellar medium of our Galaxy is highly obscuring and the distances of the stars are unknown. Also, the MCs probe a lower metallicity than the disc of our Galaxy.

Various dedicated surveys have been devoted to observe the AGB population of the MCs: the Magellanic Clouds Photometric Survey (MCPS; Zaritsky et al. 2004), the Two Micron All Sky Survey (2MASS; Skrutskie et al. 2006), the Deep Near Infrared Survey of the Southern Sky (DENIS; Epchtein et al. 1994), the Surveying the Agents of a Galaxy's Evolution Surveys with the *Spitzer telescope* for the LMC (SAGE–LMC; Meixner et al. 2006) and the SMC (SAGE–SMC; Gordon et al. 2011), and *HERschel* Inventory of The Agents of Galaxy Evolution (HERITAGE; Meixner et al. 2010, 2013).

These surveys have produced a wealth of data on AGB stars, which can be used to compare to the results of theoretical calculations. To reproduce the observed IR colours, which are sensitive to the amount of dust formed in the circumstellar envelope, some research groups couple the description of the internal star with the dust formation process in the wind. This approach was first set up by the Heidelberg team (Ferrarotti & Gail 2001, 2002, 2006) and later used by other independent investigators (Ventura et al. 2012a,b, 2014; Di Criscienzo et al. 2013; Nanni et al. 2013a,b, 2014).

Against this background, we have started a research project aimed at constraining the uncertain physics of AGB evolution, by focusing our attention on the most obscured AGB stars in the MCs.

This study follows Marigo et al. (2008), who built theoretical isochrones which included the AGB phase and extended the isochrones to the IR bands. Here we take a step forward by relaxing some of the assumptions made by Marigo et al. (2008). These include determining the expansion velocity of the wind and the final dust-to-gas ratio, and we model the AGB phase by the full integration of the stellar structure equations, rather than using a synthetic approach. We base our analysis on AGB models calculated from two independent stellar evolution codes which made a significant contribution to the literature of AGB stars over the past couple of decades: MONASH (Frost & Lattanzio 1996) and ATON (Ventura et al. 1998). The two codes have been developed and updated independently and include numerous differences between each other in the numerical structure and in the physical ingredients used. This procedure provides us with a much more complete and critical analysis because (a) it adds robustness to common findings; (b) the discrepancy between results provides an estimate of the uncertainty associated with that result; and (c) the comparison with the observations may allow us to select the most appropriate description of a given phenomenon (e.g. the treatment of convective borders).

In the first paper of this series (Ventura et al. 2015a), we focused on oxygen-rich stars in the LMC with the brightest IR emission, interpreted as the progeny of 5–6 $M_{\odot}$ stars experiencing hot bottom burning (HBB).

In this paper, we turn to the carbon star population in the MCs. The goal of the present investigation is to use the sample of numerous C-rich AGB stars to reconstruct the various stages of their evolutionary history. In particular, we are interested in studying the amount of carbon accumulated in the external mantle and the rate at which their envelope has been gradually lost by stellar winds.

We will preferentially concentrate on the C-stars with the largest degree of obscuration, for which the mass and chemical composition of the progenitors can be established; this makes the comparison with the models easier and more reliable.

The paper is organized as follows. Section 2 presents an overview of the observations of the AGB population of the MCs, with a summary of the interpretative analysis proposed so far. The physical ingredients used to calculate the evolutionary sequences presented here and the method followed to describe the dust formation process and to produce synthetic spectra are given in Section 3. Section 4 presents the results concerning the main evolution and dust properties of the stars currently evolving through the C-rich AGB phase in the MCs. The comparison between the AGB stars with the largest degree of obscuration and the results from theoretical models is given in Section 5, while Section 6 discusses our interpretation in terms of other observational parameters as well as future observations to test it. Conclusions are presented in Section 7.

2 AGB STARS IN THE MCs

The results from the surveys MCPS, 2MASS and DENIS have been used to derive information on the internal structure and on the efficiency of the mechanisms that are altering the surface chemical composition of AGB stars.

Studies focused on the interpretation of the luminosity function of carbon stars in the LMC and SMC have provided important information on the efficiency of TDU and the core mass at which TDU begins (Groenewegen & de Jong 1993; Marigo, Girardi & Bressan 1999; Karakas, Lattanzio & Pols 2002; Izzard et al. 2004; Stancliffe, Izzard & Tout 2005; Marigo & Girardi 2007).

The mid-infrared (mid-IR) *Spitzer* data, combined with near-IR 2MASS photometry, have been extensively used to derive the main properties of the stars observed, specifically the luminosity, the rate of mass-loss and the dust injection rate (Groenewegen et al. 2007; Srinivasan et al. 2009; Riebel et al. 2010, 2012; Boyer et al. 2011, 2012; Srinivasan, Sargent & Meixner 2011). Various methods have been proposed to classify the observed stars and separate carbon stars from their oxygen-rich counterparts (Cioni et al. 2000a, 2006; Cioni, Habing & Israel 2000b). The stars with the highest degree of obscuration have been traditionally referred

Downloaded from http://mnras.oxfordjournals.org/ at NASA Goddard Space Flight Ctr on May 24, 2016

to as 'extreme' (Blum et al. 2006), owing to their extremely red IR colours and the uncertain surface chemical composition.

In a series of papers (Dell'Agli et al. 2014, 2015a,b), we tackled the problem of interpreting the IR observations of the MC AGB star population by confronting the observational evidence with results of full AGB evolutionary models. The models also account for dust formation in the circumstellar envelope. The latter ingredient is mandatory because radiation from the central object is reprocessed to longer, IR wavelengths by dust.

Based on the results by Dell'Agli et al. (2015a), Ventura et al. (2015a) performed an extensive exploration of the various inputs used to build AGB evolutionary sequences of oxygen-rich intermediate-mass stars in the LMC. The study, which used results from different evolutionary codes, found that the expected position in the various IR colour–colour planes occupied by oxygen-rich AGB stars during the phase with the strongest obscuration is practically independent of the details of AGB modelling.

In this paper, we turn our attention to the C-star population in the LMC and SMC. Dell'Agli et al. (2014) characterized the AGB stars populating the diagonal band in the CCD of the two galaxies, extending to $[3.6]-[4.5]\sim3$ (LMC; Srinivasan et al. 2011) and $[3.6]-[4.5]\sim1.2$ (SMC; Boyer et al. 2011), as carbon stars (see also Dell'Agli et al. 2015a,b). The scenario proposed by Dell'Agli et al. (2014) is that the observed bands represent obscuration sequences: the stars move across the diagonal band as they become more enriched in carbon, owing to the effects of TDU. The subsequent investigations by Dell'Agli et al. (2015a,b) followed a population synthesis approach, which allowed us to determine the expected distribution of stars in the colour–colour and colour–magnitude planes obtained with the *Spitzer* bands. These studies are based on the star formation history (SFH) of the MCs by Harris & Zaritsky (2004, 2009) and on the evolutionary times of stars of various mass and metallicity, reported in table 1 in Dell'Agli et al. (2015a).

One general result is that the regions of the observational planes where highly obscured carbon stars are found are not well populated. This is because the evolutionary time-scales get shorter as the star becomes enriched in carbon, owing to the considerable increase in the rate of mass-loss. This has important consequences on the (current) mass distribution of the carbon stars observed. All the stars with initial mass in the range $\sim$1.25–3 $M_\odot$ evolve as carbon stars from a given stage of the evolution until the removal of the envelope, where the final stellar mass is $\sim$0.6 $M_\odot$. On the other hand, for the reasons given above, the very final evolutionary phases have a very short duration. The combination of these two factors makes the mass distribution of the LMC to peak around $\sim$1.3–1.4 $M_\odot$, in nice agreement with the analysis based on pulsation periods by Boyer et al. (2015).

Dell'Agli et al. (2015a) found that in the LMC the C-rich AGB stars with the reddest IR colours formed during the $\sim$300-Myr-long epoch of high star formation, which occurred $\sim$500 Myr ago, when most of the stars formed from gas with metallicity $Z=0.008$. An age of $\sim$300–500 Myr corresponds to stars with initial masses $\sim$2.5–3 $M_\odot$.

By applying to the SMC the same population synthesis analysis, Dell'Agli et al. (2015b) found that the stars exhibiting the largest obscuration descend from $\sim$1.5 $M_\odot$ stars, formed $\sim$2 Gyr ago, when the dominant metallicity of the interstellar medium was $Z=0.004$. Contrary to the LMC, only a negligible fraction of stars descending from $\sim$2.5–3 $M_\odot$ objects are expected to evolve nowadays through the very final AGB phases of highest obscuration, because the star formation rate of the SMC exhibits a much narrower peak than the LMC at $\sim$500 Myr ago.

We will focus on these masses and metallicities in the following sections.

3 NUMERICAL AND PHYSICAL INPUTS

3.1 Stellar evolution models

This work is based on evolutionary sequences calculated with the ATON code (Ventura et al. 1998) and with the Monash version of the Mount Stromlo Stellar Structure Program (MONASH; Frost & Lattanzio 1996). Exhaustive discussions on the numerical and physical input adopted are found in the papers by Ventura et al. (2013) and Karakas (2010), which also provide a detailed description of the chemical and physical properties of the AGB evolution of these stars.

The main differences between the two sets of models are the treatment of convection, the description of mass-loss and the calculation of molecular opacities in the low-temperature region of the envelope.

(i) In the ATON code, the convective instability is described by means of the full spectrum of turbulence model developed by Canuto & Mazzitelli (1991), whereas in the MONASH case the traditional mixing length theory is used.

(ii) The ATON sequences are calculated by coupling nuclear burning and mixing of chemicals in a diffusive-like scheme. Overshoot of convective eddies into radiatively stable regions is described by means of an exponential decay of velocities from the convective/radiative interface, fixed by the Schwarzschild criterion. The e-folding distance is assumed to be $0.002H_{\rm p}$ (where $H_{\rm p}$ is the pressure scaleheight calculated at the formal boundary of convection), in agreement with the calibration based on the observed luminosity function of carbon stars in the LMC, given by Ventura et al. (2014). The MONASH models of Karakas (2010) assume instantaneous mixing and no overshoot beyond the formal Schwarzschild boundary is applied. However, the MONASH models implement an algorithm to search for a neutrally stable point (e.g. Lattanzio 1986), which has been shown to increase the amount of TDU relative to models without (Frost & Lattanzio 1996). Note that in low-mass AGB models the amount of TDU found by this algorithm is still less than required to match the C/O transition luminosity of MC AGB stars and some formal overshoot had to be applied (Kamath, Karakas & Wood 2012).

(iii) The mass-loss rate for oxygen-rich models in the ATON case is determined via the Blöcker (1995) treatment; for carbon stars ATON uses the results from the Berlin group (Wachter et al. 2002, 2008). MONASH models rely on the classic description by Vassiliadis & Wood (1993).

(iv) In the ATON sequences, molecular opacities in the low-temperature regime (below 10^4 K) are calculated by means of the AESOPUS tool (Marigo & Aringer 2009). The opacities are suitably constructed to follow the changes in the chemical composition of the envelope, particularly of the individual abundances of carbon, nitrogen and oxygen. The MONASH models from Karakas (2010) include an approximate treatment for the molecular opacities (in particular CN, CO, H_2O and TiO) using the formulations from Bessell et al. (1989) with the corrections by Chiosi, Wood & Capitanio (1993). These fits do include some compositional dependence, but do not account for large variations in the CNO species.

Downloaded from http://mnras.oxfordjournals.org/ at NASA Goddard Space Flight Ctr on May 24, 2016

3.2 Dust formation in the winds of AGB stars

The growth of dust particles in the circumstellar envelope is described following the pioneering explorations by the Heidelberg group (Gail & Sedlmayr 1985, 1999; Ferrarotti & Gail 2001, 2002, 2006; Zhukovska, Gail & Trieloff 2008). The wind is assumed to expand isotropically from the surface of the star; the velocity is held constant until gas molecules enter the region where condensation into dust particles is favoured. As far as a minimum amount of dust is formed, the results are independent of the adopted initial velocity.

The model is based on the equation of momentum conservation and on a differential relation for the radial variation of the optical depth:

$$v\frac{\mathrm{d}v}{\mathrm{d}r} = -\frac{GM}{r^2}(1-\Gamma) \tag{1}$$

$$\frac{\mathrm{d}\tau_L}{\mathrm{d}r} = -\rho k\frac{R^2}{r^2}, \tag{2}$$

where $\Gamma = \frac{kL}{4\pi cGM}$ accounts for the effects of radiation pressure on dust grains, while k is the extinction coefficient.

The description of the wind is completed by the equation giving the radial variation of temperature and by the mass continuity relation:

$$T^4 = \frac{1}{2}T_{\rm eff}^4\left[1-\sqrt{1-\frac{R^2}{r^2}}+\frac{3}{2}\tau_L\right] \tag{3}$$

$$\dot{M} = 4\pi r^2\rho v. \tag{4}$$

Here we focus on carbon-rich environments, where the surface carbon abundance exceeds oxygen. In this case, the two main dust species formed are solid carbon (C) and silicon carbide (SiC). The condensation reactions by which the two species form are, respectively, $C_2H_2 \rightarrow 2C(s) + H_2$ and $2Si + C_2H_2 \rightarrow 2SiC(s) + H_2$ (see, e.g., Ferrarotti & Gail 2006). The condensation temperatures are 1100 K (C) and 1400 K (SiC). The growth rate of dust grains ($\mathrm{d}a_{\rm C}/\mathrm{d}t$ and $\mathrm{d}a_{\rm SiC}/\mathrm{d}t$) is proportional to the least abundant among the species involved in the condensation reactions, namely C_2H_2 and silicon. Considering the high stability of CO and SiS molecules, we have

$$\frac{\mathrm{d}a_{\rm C}}{\mathrm{d}t} \propto n_{\rm C_2H_2} \propto (1-f_{\rm C})n_{\rm C} - n_{\rm O} - (1-f_{\rm SiC})n_{\rm Si} \tag{5}$$

$$\frac{\mathrm{d}a_{\rm SiC}}{\mathrm{d}t} \propto (1-f_{\rm SiC})n_{\rm Si} - n_{\rm S}. \tag{6}$$

In the above equations, $f_{\rm C}$ ($f_{\rm SiC}$) indicates the fraction of carbon (silicon) molecules condensed into dust particles.

SiC is the most stable species and forms at higher temperatures, thus closer to the surface of the star. Equation (6) indicates an upper limit to the growth of SiC particles, reached when the fraction of silicon molecules condensing into SiC approaches $f_{\rm SiC} = 1 - n_{\rm S}/n_{\rm SiC} \sim 0.55$. Because neither silicon nor sulphur undergoes significant variations along the life of stars of intermediate mass, this quantity remains constant during the AGB phase.

While the formation of SiC grains is important for the IR properties of the spectral energy distribution (SED) of AGB stars, it does not influence the dynamical status of the wind. This is because SiC particles are extremely transparent to electromagnetic radiation and thus do not contribute to the acceleration of the wind via radiation pressure.

Solid carbon is less stable than SiC; therefore, the zone where the formation of carbon grains occurs is more external than the region where SiC particles begin to form. Because the surface carbon abundance is generally much higher than that of silicon, contrary to SiC, no saturation in the carbon dust formation process occurs. The only exception is at the very beginning of the C-rich phase, when the carbon excess with respect to oxygen is very small, which prevents the formation of significant quantities of carbon dust (see equation 5).

However, because of the very large values attained by the extinction coefficient of solid carbon grains, the growth of these particles is commonly halted by the considerable expansion of the wind, which determines a fast drop in the gas density, according to equation (4).

We may safely assume in this case (e.g. equation 5) that the key quantity is the density of C_2H_2 molecules.[1] The density of C_2H_2 in turn depends on the surface carbon mass fraction and on the density of the wind in the region where condensation occurs, i.e. the zone where the temperature is $T_{\rm C} = 1100$ K; we refer to the density of this region as $\rho_{\rm C}$.

Because the typical distance from the surface at which solid carbon forms is $\sim 10\,R_*$, we may safely expand equation (3) assuming that $R_*/r \ll 1$, to obtain

$$(R_*/r)^2 \sim 4(T_{\rm C}/T_{\rm eff})^4 - 4/3\tau_L. \tag{7}$$

The combination of equations (4) and (7) leads to

$$\rho_{\rm C} \sim \frac{\dot{M}}{v}\left[\frac{T_{\rm C}^4}{L} - \frac{\tau_L}{12\pi\sigma R_*^2}\right]. \tag{8}$$

The first term on the right-hand side of equation (8) is dominant. Therefore, the number of C_2H_2 molecules available to form solid carbon is determined by the carbon mass fraction, X(C) and the $\dot{M}/L$ ratio.

We may therefore conclude that the winds of carbon stars have the following stratification.

(i) SiC forms in an internal zone, at a temperature of $\sim$1400 K. In most cases, the growth of SiC particles is halted by saturation, which occurs when the fraction of gaseous silicon condensing into dust approaches $\sim$55 per cent (see discussion in the previous section). The wind is modestly accelerated by formation of SiC, because this species is highly transparent to radiation.

(ii) Solid carbon particles form in more external regions, where the temperature is $\sim$1100 K. In this case, the wind is greatly accelerated owing to the high values of the extinction coefficient of carbon dust. The factors mostly relevant to formation of solid carbon are the $\dot{M}/L$ ratio and the surface carbon mass fraction.

3.3 Synthetic spectra

To determine the magnitudes in the *Spitzer* bands used in the present analysis, we follow the same approach as used in Ventura et al. (2015a) and discussed in detail in Dell'Agli et al. (2015a). Based on the values of mass, luminosity, effective temperature, mass-loss rate and surface chemical composition calculated from the MONASH and ATON codes, we apply the model of dust formation described in Section 3.2 to determine the size of the dust grains formed and the optical depth (here we use the value at 10 μm, τ_{10}).

[1] This is consistent with mid-IR spectroscopic observations of Galactic and MC AGB stars, which show that C_2H_2 is very abundant in their circumstellar envelopes (e.g. van Loon, Zijlstra & Groenewegen 1999; Yang, Chen & He 2004; Lagadec et al. 2007; van Loon et al. 2008).

Downloaded from http://mnras.oxfordjournals.org/ at NASA Goddard Space Flight Ctr on May 24, 2016

These ingredients are used by the code DUSTY (Nenkova, Ivezić & Elitzur 1999) to calculate the synthetic spectra of each selected point along the evolutionary sequence. The magnitudes in the various bands are obtained by convolution with the appropriate transmission curves. DUSTY needs as input parameters the effective temperature of the star, the radial profile of the density of the gas and the dust composition of the wind, in terms of the percentage of the various species present and of the size of the dust particles formed. All these quantities are known based on the results of stellar evolution and of the description of the wind.

4 CARBON STARS IN THE MCs: EVOLUTION AND DUST PROPERTIES

We focus now on the stars that account for most of the C-star population in the LMC and SMC. For the LMC we consider models of initial mass ∼2.5–3 $M_\odot$ and metallicity $Z = 8 \times 10^{-3}$. To compare models with the same core mass, while in the ATON case we show models of initial masses 2.5 and 3 $M_\odot$, in the MONASH case we present the 2.25 and 3 $M_\odot$ models; this is due to a slight difference in the mass versus core mass relationships found with the two codes in the range of masses close to the limit to experience the helium flash. For the SMC, we analyse the evolution of ∼1.5 $M_\odot$ stars of metallicity $Z = 4 \times 10^{-3}$.

4.1 Physical properties of carbon stars

The evolution of these models is shown in Fig. 1, where we plot the luminosity, effective temperature, mass-loss rate and surface carbon abundance as a function of time from the beginning of the thermally pulsing AGB phase.

The top-left panel of Fig. 1 shows that the ATON and MONASH models evolve at similar luminosities, an indication that the core masses are similar. Note that in this case we do not expect any effect of convection modelling on the behaviour of luminosity, because stars in this range of mass do not experience HBB. This is at odds with the analysis by Ventura et al. (2015a), where the ATON and MONASH models of 5–6 $M_\odot$ stars were shown to evolve at different luminosities. The only meaningful difference is the duration of the whole AGB phase, which is systematically longer in the MONASH models; we will come back to this point shortly. The duration of the AGB phase is not monotonic with mass: the 2.5 $M_\odot$ model evolves for a longer time compared to their 1.5 and 3 $M_\odot$ counterparts. This is because the relationship between the core mass at the beginning of the AGB phase and the initial mass of the stars has a minimum at ∼2.5 $M_\odot$, which makes the growth of the luminosity of the 2.5 $M_\odot$ model in the initial AGB phases slower than in the other cases.

In the phases before the C-star phase is reached, the effective temperatures of models of the same mass are similar in the MONASH and ATON cases (see the top-right panel of Fig. 1). After the C/O ratio exceeds unity, the effect of the different low-temperature opacities takes over: the ATON models, owing to the expansion of the external regions triggered by the increase in the opacity, evolve to lower temperatures, down to ∼2000 K, whereas in the MONASH models we find $T_{\rm eff} > 2400$ K. This effect is extensively discussed in Ventura & Marigo (2009, 2010).

The difference in the surface temperature has a direct effect on the rate of mass-loss. As shown in the bottom-left panel of Fig. 1, $\dot{M}$ exceeds 10^{-4} $M_\odot$ yr^{-1} in the ATON models of $Z = 8 \times 10^{-3}$, whereas in the MONASH case it is ∼3–4 times smaller; in the 1.5 $M_\odot$ model of metallicity $Z = 4 \times 10^{-3}$ the difference is smaller (2×10^{-5} and 3×10^{-5} $M_\odot$ yr^{-1} in the MONASH and ATON models, respectively). This is not only due to the more expanded, hence less gravitationally bound, configurations of lower $T_{\rm eff}$'s models; a further reason for the higher $\dot{M}$'s of the ATON models is the use of the formulation by Wachter et al. (2002, 2008), which favours large rates of mass-loss in carbon-rich, low-$T_{\rm eff}$ stars. The rate of mass-loss in the ATON models is generally larger than in the MONASH cases also during the early AGB phases. This is due to the differences between the Blöcker (1995) and Vassiliadis & Wood (1993) formulae for M stars. This is not a major problem here because little mass is lost during the oxygen-rich phase of these stars and, as will be shown in the following, the amount of dust formed during these evolutionary phases is negligible in comparison to the late evolutionary phases, when the stars are carbon-rich.

4.2 The change in the surface chemistry

Concerning the surface chemistry, we show in the bottom-right panel of Fig. 1 the variation of the carbon abundance in the same models shown in the other panels. The most relevant difference between the results found with the two evolution codes is found in the 3 $M_\odot$ case, for which the MONASH and ATON models reach final carbon mass fractions of $X_{\rm C} = 0.0185$ and 0.01, respectively. This situation is reversed in lower mass models; indeed in the 1.5 $M_\odot$ ATON case the final surface carbon is $X_{\rm C} \sim 0.007$, a factor of 2 higher than MONASH. This is because the MONASH models do not show very efficient dredge-up at the minimum mass for C-star production, a problem that has been discussed extensively in Kamath et al. (2012) and Karakas, Campbell & Stancliffe (2010). The 1.5 $M_\odot$ model only dredges up 0.0096 $M_\odot$ of material from the He-intershell, with a minimum core mass for TDU of 0.6 $M_\odot$. Kamath et al. (2012) found that the minimum mass for TDU in LMC AGB stars should be lower, at 0.58 $M_\odot$, indicating that convective overshoot should probably be applied (see also, e.g., Marigo et al. 1999). To reach surface carbon mass fractions $X_{\rm C} > 0.005$, an extra-mixing zone extending over two pressure scaleheights below the base of the convective envelope needs to be applied. This is entirely consistent with the analysis by Kamath et al. (2012), who invoked an overshoot of similar extension to match the observations of AGB stars in MC clusters.

These dissimilarities between the results obtained with the two evolution codes are not surprising, given the considerable sensitivity of the carbon enrichment of the surface layers to the details of the treatment of convective borders, as thoroughly documented in the literature (Karakas & Lattanzio 2014).

4.3 Dust formation in the circumstellar envelope

The changes in the SED of AGB stars are correlated with evolution properties. This reflects the variation of the main physical parameters (e.g. mass-loss) and of the quantity of dust in the circumstellar envelope.

Fig. 2 shows the evolution of the size of the dust grains formed (left-hand panel) and the optical depth at wavelength $\lambda = 10$ μm, τ_{10}, for the same models shown in Fig. 1. For clarity, we only show the dimension of the dust particles formed in greater quantities, which provide the dominant contribution to the acceleration of the wind, i.e. olivine (oxygen-rich phases) and solid carbon (C-stars). τ_{10} is plotted on a logarithmic scale, which allows us to discuss the early AGB phase, which is otherwise undetectable on a linear scale plot. On the abscissa, we show the surface mass fraction of carbon, which increases during the AGB phase.

Downloaded from http://mnras.oxfordjournals.org/ at NASA Goddard Space Flight Ctr on May 24, 2016

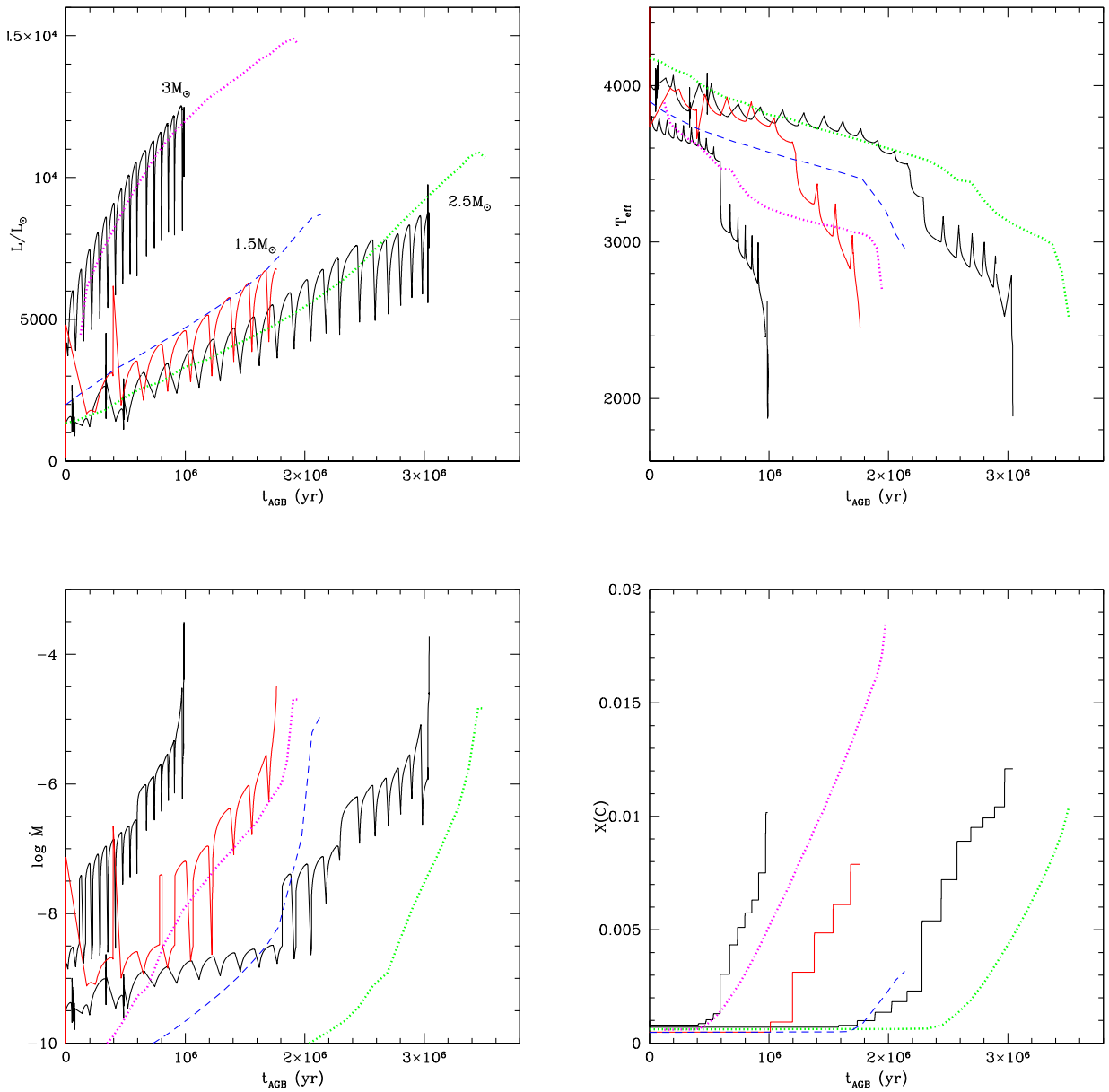

Figure 1. The variation of luminosity (top-left panel), effective temperature (top-right), rate of mass-loss (bottom-left) and surface carbon mass fraction (bottom-right) during the AGB phase of models of various mass and metallicity, calculated with MONASH and ATON codes. The ATON models of initial mass 2.5, 3 $M_\odot$ and metallicity $Z = 8 \times 10^{-3}$ are indicated with solid black lines, whereas the ATON 1.5 $M_\odot$, $Z = 4 \times 10^{-3}$ evolutionary sequence is plotted with a solid red track. The dotted magenta and green lines indicate the evolution of the MONASH models of metallicity $Z = 8 \times 10^{-3}$ and initial mass, respectively, 3 and 2.25 $M_\odot$; the MONASH model of mass 1.5 $M_\odot$ and $Z = 4 \times 10^{-3}$ is indicated with a dashed blue line. Note that while the ATON tracks show the whole AGB evolution, including the thermal pulses, the MONASH lines are limited to the inter-pulse phases.

The following results are in common between the MONASH and ATON models.

(i) Little dust formation occurs until the C/O ratio is close to unity. As shown in Fig. 2, the olivine grains barely exceed a nanometre size and the optical depth is very small. The SED of the star is unaffected by dust during these phases. This holds independently of mass and metallicity.

(ii) The quantity of carbon dust formed increases during the subsequent C-star evolution, as confirmed by the rise of the grain size and τ_{10}, shown in Fig. 2. This can be understood based on the discussion in Section 3.2, because both factors affecting formation of carbonaceous dust, namely the surface carbon abundance and the $\dot{M}/L$ ratio, increase after becoming C-rich (see Fig. 1).

(iii) The amount of dust formed in the winds of the ∼1.5 $M_\odot$ star is significantly smaller than in their counterparts of higher mass. This is because the 2.5–3 $M_\odot$ models, particularly during the final AGB phases, attain a higher surface carbon abundance, which in turn leads to lower effective temperatures and higher rates of mass-loss; this can be clearly seen in Fig. 1.

4.4 Thermodynamic and chemical structure of the wind

To understand how the conditions in the wind evolve, we show in Fig. 3 the stratification of the circumstellar envelope in three distinct

Downloaded from http://mnras.oxfordjournals.org/ at NASA Goddard Space Flight Ctr on May 24, 2016

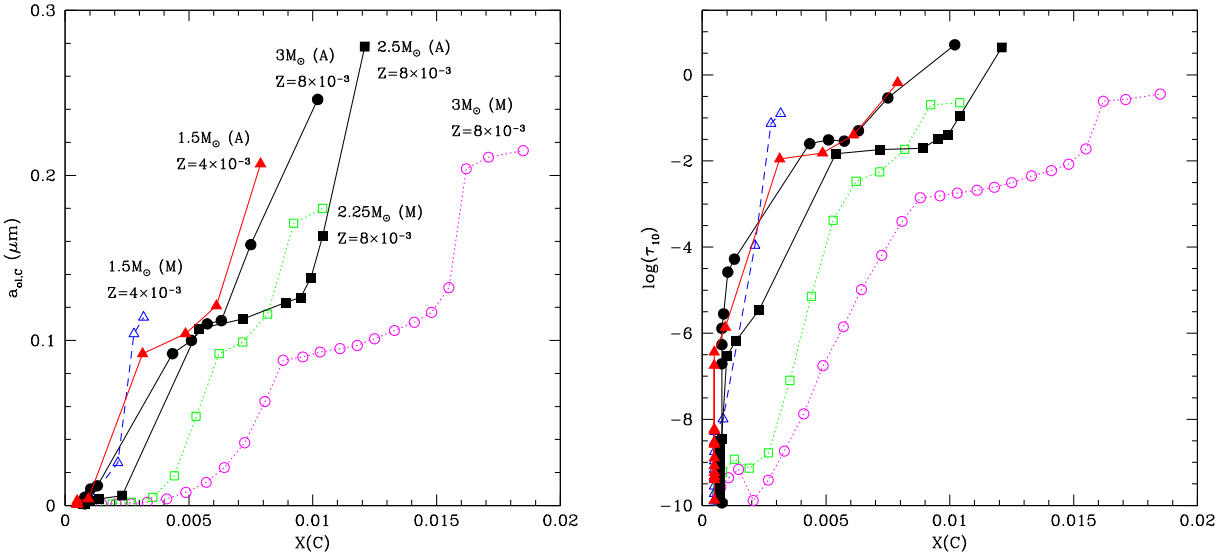

Figure 2. The variation of the size of the olivine (oxygen-rich phases) and solid carbon (carbon stars) dust grains (left-hand panel) and of the optical depth at 10 μm (right) in the same models shown in Fig. 1. On the abscissa, we show the surface carbon abundance, increasing during the AGB phase. Symbols along the tracks in the left-hand panel indicate the initial mass and whether the MONASH (M) or ATON (A) code was used for the calculation.

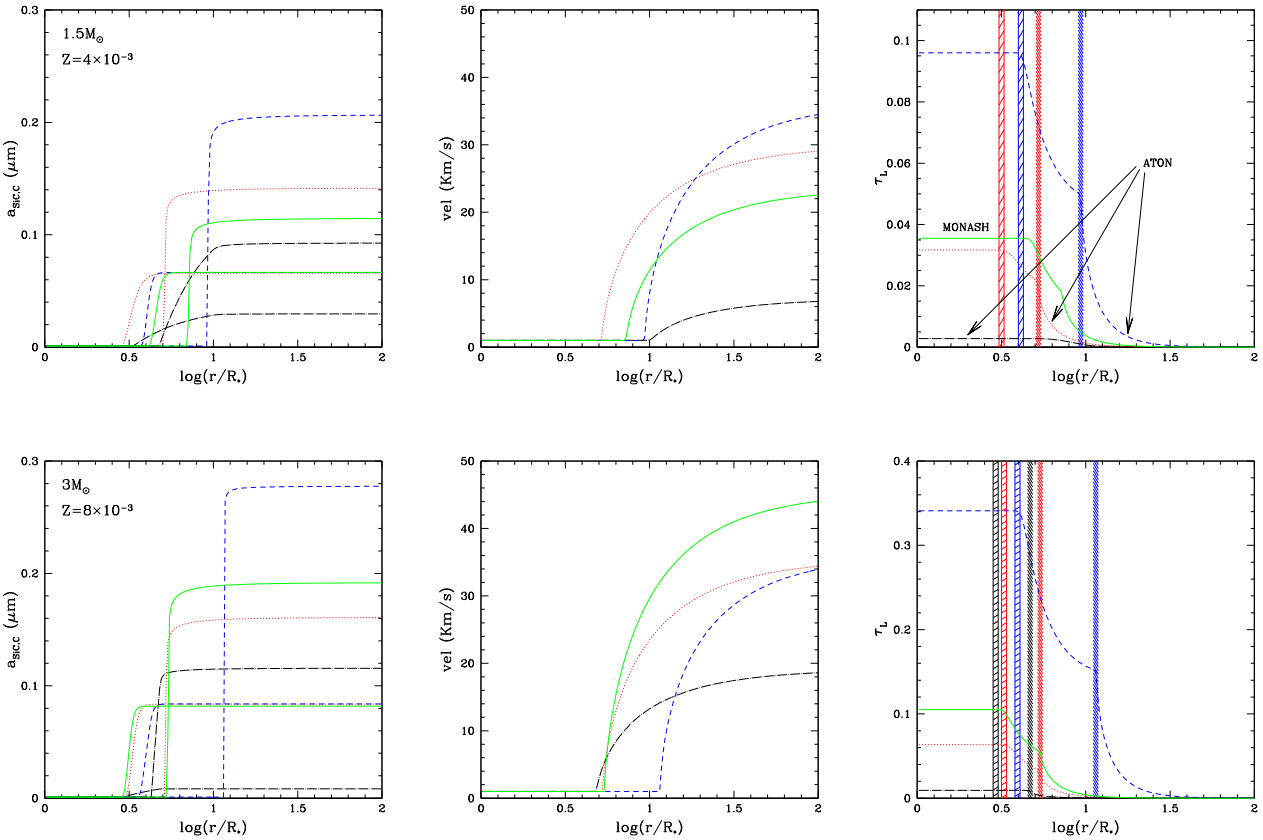

Figure 3. The radial stratification of the size of SiC and carbon grains (left-hand panels), wind velocity (middle) and τ_L (right) in different phases during the AGB evolution of models of initial mass 1.5 $M_\odot$ (top) and 2.5 $M_\odot$ (bottom). On the abscissa, we show the distance from the surface of the star, on a logarithmic scale, measured in stellar radii units. Black dot–dashed, red dotted and dashed, blue tracks refer to ATON models taken, respectively, at the beginning of the C-star phase, in an intermediate stage after becoming C-star and at the end of the AGB evolution. Solid green lines correspond to MONASH models of initial mass 1.5 $M_\odot$ (top) and 3 $M_\odot$ (bottom), taken in the final evolutionary phases. The shaded regions outlined in the right-hand panels indicate the zones where formation of SiC and solid carbon dust occurs.

Downloaded from http://mnras.oxfordjournals.org/ at NASA Goddard Space Flight Ctr on May 24, 2016

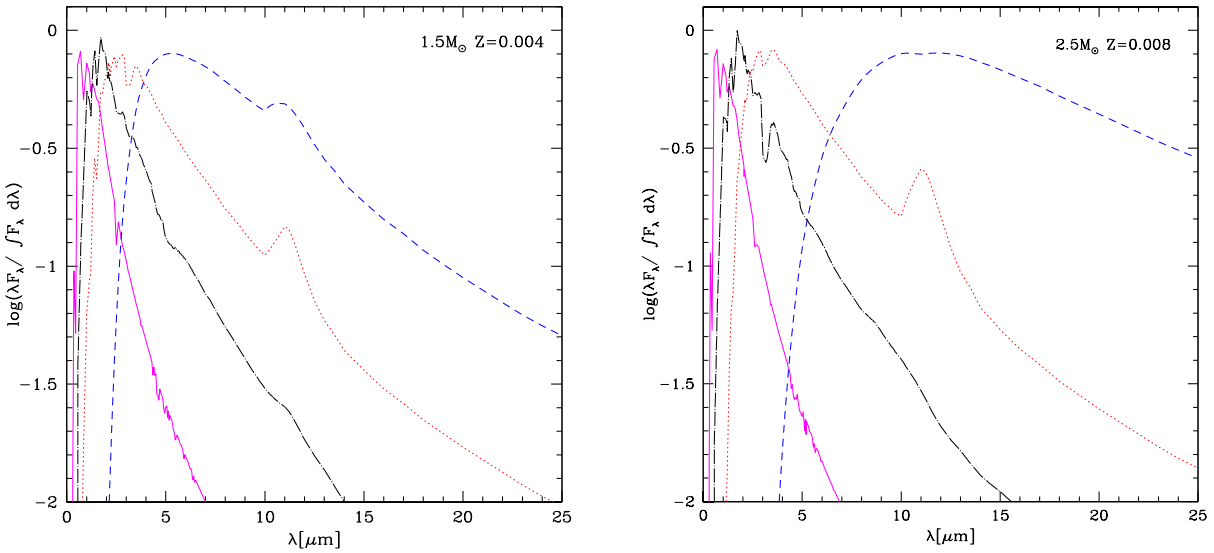

Figure 4. The evolution of the SED of low-mass stars evolving to the C-star stage during the AGB phase. The solid magenta lines correspond to the SED at the beginning of the AGB phase, when the stars are still oxygen-rich. Dot–dashed, dotted and dashed tracks correspond to the same model as in Fig. 3.

stages of the carbon star phase of the 1.5 $M_\odot$, $Z = 4 \times 10^{-3}$ (top panel) and the 2.5 $M_\odot$, $Z = 8 \times 10^{-3}$ ATON models. The plots illustrate conditions at the beginning of the AGB phase, the very end of the AGB evolution and an intermediate phase. In the same figure, we also show the MONASH models of masses 1.5 and 3 $M_\odot$ during the final AGB phases. The panels of the figure show the radial distribution of the grain sizes of SiC and solid carbon, the velocity of the wind and τ_L, the quantity entering equations (2) and (3).

Formation of SiC occurs in an internal zone, ∼2–3 stellar radii away from the surface, where the temperature is $T \sim 1400$ K. Because SiC is highly transparent to stellar radiation, the velocity of the wind stays constant in the region of SiC formation. At the very beginning of the carbon star phase, SiC is produced in modest quantities, with grains of a few nanometres in size. In more advanced phases saturation condition occurs, the dimension of SiC grains grows to 0.065 and 0.081 μm in the 1.5 and 2.5 $M_\odot$ cases, respectively. This is because silicon in the envelope is either locked into SiS molecules or condensed into SiC particles. The difference in the SiC grain size is due to the dependence of the surface silicon abundance on initial metallicity.

Formation of carbon grains occurs ∼7–10 stellar radii away from the surface, where the temperature is $T \sim 1100$ K. Carbon is produced in greater quantities compared to SiC, owing to the higher availability of carbon molecules in comparison to silicon. The formation of carbon dust is accompanied by the acceleration of the wind. The location of the carbon condensation zone is gradually shifted outwards during the AGB evolution; this is because the slope of the $T(r)$ relation is smaller for lower effective temperatures and the higher τ_L also result in pushing out the region where $T \sim 1100$ K (see equation 3). The typical size of the carbon grains formed, a_C, is of the order of 0.1-0.2 μm and increases during the AGB evolution. In the final evolutionary phases of the 2.5 $M_\odot$ model, we find $a_C \sim 0.3$ μm, whereas we get a maximum dimension $a_C \sim 0.2$ μm in the 1.5 $M_\odot$ case.

In the comparison between the SiC and solid carbon dust formed, we note that the amount of SiC, after saturation conditions occur, stays constant during the AGB evolution. On the other hand, larger and larger quantities of solid carbon grains are formed as the star accumulates carbon in the surface regions. Therefore, we expect that the SiC/C ratio decreases during the AGB evolution (see Fig. 4 and Section 6).

The velocity reached by the wind also increases during the evolution of these stars, spanning the range 10–50 km s^{-1}.

4.5 An overview of MONASH and ATON results

The comparison between the MONASH and ATON results allows us to study the main factors affecting carbonaceous dust formation in AGB stars.

The evolution of the IR properties of these stars is strongly related to the amount of dust formed. As discussed in Section 3.2, formation of solid carbon is determined by the surface carbon abundance and the $\dot{M}/L$ ratio. The former is relevant at the beginning of the C-star phase, as confirmed by the steep slope of the a_C versus X(C) and τ_{10} versus X(C) relations shown in Fig. 2. This is because the growth rate of carbon dust is proportional to the density of C_2H_2 molecules, which in turn is given by the carbon excess with respect to oxygen (see equation 5). For small carbon abundances, even a small change of X(C) favours a high percentage increase in $n_{C_2H_2}$, which results in a significant rise in the growth rate of carbon grains. After the surface carbon exceeds $X(C) \sim 5 \times 10^{-3}$, the relative weight of this factor diminishes, because any additional change will result in a smaller percentage increase in the number density of C_2H_2 particles; the $\dot{M}/L$ ratio plays a dominant role here.

Fig. 2 shows that at the end of the AGB evolution, higher values of τ_{10} are reached in the ATON models. For $M = 1.5\,M_\odot$ we find $\tau_{10} = 0.1$ in the MONASH model, whereas we obtain $\tau_{10} = 0.7$ in the ATON case. In this case, the star reaches relatively small carbon abundances, $X(C) < 7 \times 10^{-3}$. Following the above discussion, we know that this is the domain most affected by the carbon content. The ATON model produces more dust than MONASH (see the left-hand panel of Fig. 2), owing to the higher availability of carbon in the surface regions, as shown in the bottom-right panel of Fig. 1. The IR emission is consequently more intense in the ATON case.

Turning to models of higher mass and metallicity, we find that the 3 $M_\odot$ MONASH model evolves to $\tau_{10} \sim 1$, while the 2.5 $M_\odot$ ATON model reaches $\tau_{10} \sim 5$ at the end of the AGB phase. Stars of this

Downloaded from http://mnras.oxfordjournals.org/ at NASA Goddard Space Flight Ctr on May 24, 2016

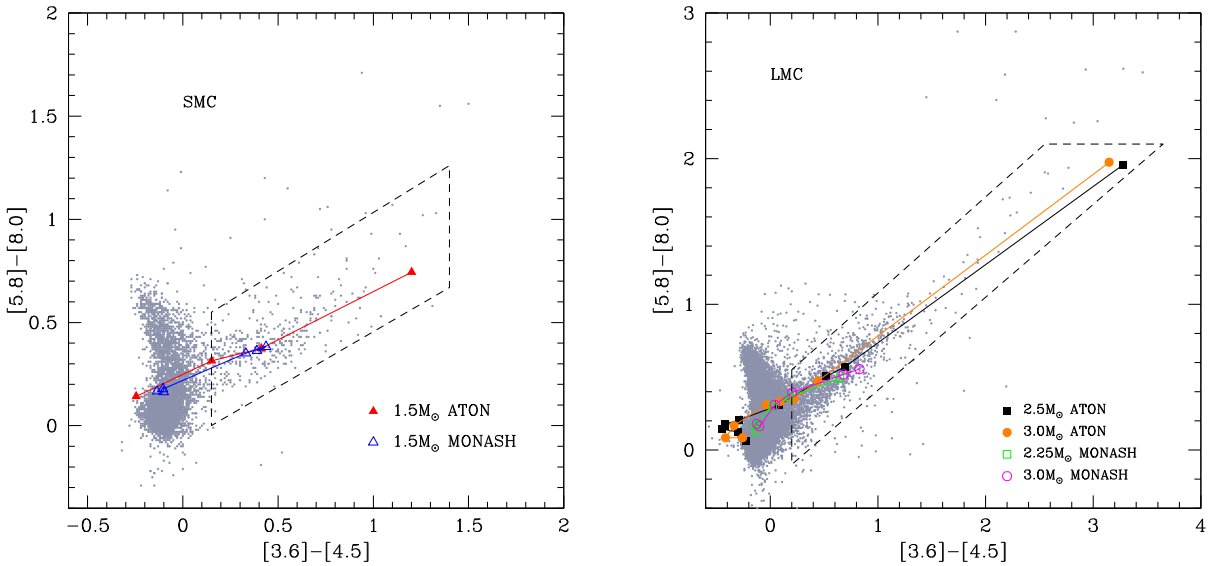

Figure 5. Left: the observations of SMC AGB stars by Boyer et al. (2011) in the colour–colour [3.6] − [4.5], [5.8] − [8.0] diagram. The 1.5 $M_\odot$ evolutionary tracks calculated with the MONASH (open blue triangles) and ATON (filled red triangles) are shown. The region delimited by the dashed lines corresponds to the zone where obscured C-stars evolve, according to the interpretation by Dell'Agli et al. (2015b). Right: observations of LMC AGB stars by Riebel et al. (2012); the evolutionary tracks correspond to MONASH models of initial mass 2.25 $M_\odot$ (open green squares), 3 $M_\odot$ (open magenta circles) and to ATON models of initial mass 2.5 $M_\odot$ (filled black squares), 3 $M_\odot$ (filled orange circles). The region delimited by dashed lines, similarly to the left-hand panel, indicates the zone populated by C-stars with an intense IR emission (Dell'Agli et al. 2015a).

mass undergo more TDU events, thus becoming more C-rich during the AGB evolution. The rate of mass-loss plays a dominant role here in affecting dust formation. This is confirmed by the comparison between the MONASH model of 3 $M_\odot$ with the ATON, 2.5 $M_\odot$ case: despite the former experiences a larger carbon enrichment (see Fig. 1), the latter reaches higher optical depths in the final phases, owing to the higher rate of mass-loss experienced.

5 *SPITZER* COLOURS OF CARBON STARS IN THE MCs

As discussed in the previous sections, the evolution of AGB stars with progenitors of mass below ∼3 $M_\odot$ is driven by the progressive enrichment of carbon in the surface regions. The SED of these stars gradually shifts to the IR, with the peak of the emission moving to longer wavelengths. This is illustrated in Fig. 4, where we show the SED of the 1.5 $M_\odot$, $Z = 4 \times 10^{-3}$ (left-hand panel) and 2.5 $M_\odot$, $Z = 8 \times 10^{-3}$ models (right), in four evolutionary phases from the beginning of the AGB evolution, with practically no dust effects, to the very final phases. At the end of the AGB phase, the SED of the 2.5 $M_\odot$ model peaks at longer wavelengths compared to the 1.5 $M_\odot$ case, for the reasons given in Section 4.3.

Fig. 5 shows AGB stars in the SMC (left-hand panel) and LMC (right) on the colour–colour ([3.6] − [4.5], [5.8] − [8.0]) plane. The regions delimited by the dashed lines are the C-star loci, according to Dell'Agli et al. (2015a,b). As discussed in Section 2, most of the obscured C-stars in the LMC descend from ∼2.5–3 $M_\odot$ progenitors, whereas in the SMC the objects with the reddest IR colours are the progeny of ∼1.5 $M_\odot$ stars. Therefore, the SEDs, corresponding to the end of the AGB phase (dashed lines), shown in Fig. 4, provide an indication of the typical colours of the most obscured AGB stars in the two galaxies. The synthetic SEDs confirm that the most obscured LMC AGB stars reach redder [3.6] − [4.5] colours than their SMC counterparts. This explains why the C-star locus in the LMC is more extended towards the red (up to [3.6] − [4.5] ∼ 3) than in the SMC ([3.6] − [4.5] ∼ 1.2)

This explanation is in contrast to the interpretation by van Loon et al. (2008), who invoked a metallicity dependence on dust formation to explain the stronger dust emission shown by carbon stars in the LMC compared to the SMC. Note that the present working hypothesis is focused on stars with the reddest colours; thus, it is not in contrast with the assumption that C-star formation is easier in the SMC because of the lower average metallicity (Sloan et al. 2008).

The overall population of C-stars in the MCs is composed of a range of masses and chemistries (Dell'Agli et al. 2015a,b), which in the general case prevents us from identifying the progenitors of the individual sources observed. To overcome this difficulty, we focus on the AGB stars populating the terminal side of the obscuration sequences of C-stars. As discussed in Section 2, each star becoming C-rich spends only a very small percentage of the AGB in the last evolutionary phase with the highest degree of obscuration. Therefore, only stars of masses and metallicities given above can be observed in such advanced evolutionary phases.

Fig. 5 shows the evolutionary tracks corresponding to the same MONASH and ATON models shown in Fig. 2. All the evolutionary sequences reproduce the diagonal band where C-stars evolve. The only discrepancy between models and the observations concerns the C-stars populating the bluest region of the CCD, centred at ([3.6] − [4.5], [5.8] − [8.0]) = (−0.1, 0.5). This group of stars present no signature of dust, consequently the synthetic spectrum is entirely determined by the GRAMS (Grid of Rsg and Agb ModelS) SED used to model the atmosphere of the central star. The reason for the difference is the absorption feature due to CO and C_3 molecules, which is not included in the GRAMS models. This is however not an issue for the present analysis, because this feature vanishes when dust is present in the circumstellar envelope (Boyer et al. 2011).

The fact that both MONASH and ATON sequences trace the observations further reinforces the main conclusions by Dell'Agli et al.

Downloaded from http://mnras.oxfordjournals.org/ at NASA Goddard Space Flight Ctr on May 24, 2016

Table 1. Main physical and dusty properties of the most obscured carbon stars in the LMC and SMC.

	[3.6] − [4.5]	τ_{10}	$a_{\rm SiC}(\mu{\rm m})$	$a_{\rm C}(\mu{\rm m})$	Age (Gyr)	$M/{\rm M}_\odot$	$L/(10^3\,{\rm L}_\odot)$	$T_{\rm eff}$	$\dot{M}/(10^{-5}\,{\rm M}_\odot\,{\rm yr}^{-1})$	Z
LMC	3.4	4.5	0.082	0.28	0.4–0.7	2.5–3	8–10	2000	15	8×10^{-3}
SMC	1.2	0.7	0.063	0.21	1.5	1.5	6–7	2500	3	4×10^{-3}

(2015a,b): the diagonal bands in the CCD of the LMC and SMC are obscuration sequences. The stars with the reddest colours correspond to those more enriched in carbon, with a larger amount of carbonaceous dust in the circumstellar envelope.

Fig. 5 shows that the ATON models nicely reproduce the observations, the evolutionary tracks reaching the terminal points of the observed sequences, both in the SMC and LMC cases. The MONASH models reproduce most of the AGB stars along the obscuration sequences, yet they do not extend to the reddest IR colours observed. This can be explained on the basis of the discussion in the previous section and of the results shown in Figs 2 and 3. For the SMC, the reason for the higher degree of obscuration reached by the ATON sequences is mainly related to the higher quantity of carbon accumulated in 1.5 $\rm M_\odot$ stars during the AGB. For the LMC case, the main reason for the discrepancy among MONASH and ATON models is the difference in the description of the low-temperature molecular opacities in C-rich environments and in the mass-loss modelling (see Section 3). These in turn affect the IR properties of the reddest AGB stars in the LMC, which reflects the mass-loss rate experienced in the final AGB phases, which in turn is related to the effective temperature.

These arguments lead us to conclude that reproducing the IR colours of the most obscured AGB stars in the SMC requires models of stars of initial mass 1.5 $\rm M_\odot$ to achieve a surface carbon abundance $X({\rm C}) > 0.005$. In order to reproduce the IR colours of the LMC AGB stars, we conclude that the main physical ingredient is the low-temperature opacities used in the calculations. The use of low-temperature opacities that follow the chemical composition of the envelope is especially important for stars with masses 2.5–3 $\rm M_\odot$, which in the last phases reach surface carbon abundances $X({\rm C}) > 0.01$. Furthermore, the description of mass-loss in C-rich environments, where significant amounts of dust form, must be based on hydrodynamical wind models including dust formation in radiative transfer equations.

We stress that the results obtained by MONASH and ATON codes are fairly similar for most of the AGB phase, for the masses and metallicities investigated here. Significant differences are found only during the two last inter-pulse phases. For this reason, the change in the physical ingredients discussed is crucial for a correct determination of the dust properties of these stars and, more generally, for the interpretation of IR properties of more complex stellar populations, where a significant population of C-stars is expected. On the other hand, we expect little effects for the other results not directly related to dust, primarily the stellar yields, which reflect the whole AGB phase.

6 WHAT DO WE LEARN FROM OBSCURED CARBON STARS IN THE MCs?

The models presented here nicely reproduce the mid-IR colours for the SMC and LMC. According to our schematization, AGB stars become more and more obscured as the carbon in the envelope increases. If this is correct, the LMC proves the ideal environment to host C-stars with an extremely intense IR emission. This is because the SFH of the LMC peaks at ∼500 Myr (Harris & Zaritsky 2009), the formation epoch of ∼2.5–3 $\rm M_\odot$ stars which are those reaching the largest abundances of carbon in the final evolutionary phases (see Fig. 1). If this understanding is confirmed, we reach the general conclusion that the degree of obscuration of the reddest stars in the LMC is the highest among C-rich AGB stars; for stars exhibiting a higher degree of obscuration, an AGB origin can be disregarded.

Table 1 reports the main properties of the individual stars which according to our interpretation populate the reddest portion of the C-star sequence in the CCD of the MCs. Observational confirmation of these quantities (in particular of the predicted radial stratification of the SiC and carbon grains) would be ideal to assess the robustness of our modelling and interpretation. Unfortunately, this is challenging with present astronomical instrumentation.

Concerning the synthetic SEDs of the stars examined here, we note that the dashed track in the right-hand panel of Fig. 4 is extremely similar to the SED of the extreme carbon star shown in the top-left panel of fig. 7 by Riebel et al. (2012), which is taken as a representative member of the group of most obscured C-stars in the LMC. Interestingly, in SMC C-rich AGB stars, the C_2H_2 and SiC features are observed to be stronger and weaker, respectively, than in the LMC stars (e.g. van Loon et al. 2006, 2008; Zijlstra et al. 2006; Lagadec et al. 2007). Indeed, our synthetic SEDs, which show an intermediate stage after becoming C-rich (red dotted lines in Fig. 4), reproduce well this observation. The 3.1 μm C_2H_2 + HCN absorption feature is stronger in a 1.5 $\rm M_\odot$ SMC AGB star than in the 3 $\rm M_\odot$ LMC case, while the opposite is seen for the ∼11.5 μm SiC feature. This is in agreement with our framework because the production of SiC (see discussion in Section 3.2) scales with the amount of silicon available at the surface, which in turn is proportional to the metallicity of the stars. Therefore, production of SiC is favoured in the LMC, because the metallicity of the C-stars in this galaxy, particularly those forming the largest quantities of dust, is generally larger than their counterparts in the SMC. On the other hand, carbon dust production is approximately independent of metallicity, because the carbon accumulated to the surface of these stars is of primary origin.

As for the global properties of these objects, Riebel et al. (2012) find that the luminosities of the most obscured C-stars in the LMC are within the range $6\times10^3 < L/{\rm L}_\odot < 10^4$, which nicely overlaps with the range of luminosities for the LMC reported in Table 1.

Concerning the mass-loss rates, Riebel et al. (2012) find that the C-stars in the LMC with the highest degree of obscuration are injecting into the interstellar medium carbonaceous dust with a rate of $\sim10^{-7}\,{\rm M}_\odot\,{\rm yr}^{-1}$. This is translated into an overall mass-loss rate of $\sim2\times10^{-5}\,{\rm M}_\odot\,{\rm yr}^{-1}$.[2] This quantity is significantly smaller than the result reported in Table 1, which is in much better agreement with the results published by Gullieuszik et al. (2012), van Loon (2006) and Groenewegen et al. (2007).

[2] To find the mass-loss rate from the dust rate, we adopted a gas/dust ratio ∼200. This is indeed what we find based on our models, with a carbon mass fraction slightly above 1 per cent and a percentage of gaseous carbon condensed into dust of ∼50 per cent.

Downloaded from http://mnras.oxfordjournals.org/ at NASA Goddard Space Flight Ctr on May 24, 2016

On the chemical side, we have seen that the conclusions we may draw for the SMC and LMC are different. In the former case, we showed that within the context of our description of the AGB and dust systems, the colours of the C-stars exhibiting the highest degree of obscuration are reproduced only if the amount of carbon accumulated at the surface exceeds ∼0.5 per cent of the total mass. This C abundance corresponds to a C/O ratio above 3. The IR colours of the most obscured LMC C-stars are however less sensitive to the surface carbon abundance than their SMC counterparts. The uncertainties affecting the degree of carbon enrichment are still significant, which is confirmed by the differences between the MONASH (surface carbon mass fraction slightly below 0.02, C/O ∼ 10) and ATON (X(C) ∼ 0.01, C/O ∼ 3) models.

The most obscured C-stars in the MCs are very faint in the optical domain but much brighter in the near-IR. Thus, the best observational way to test the different nature (i.e. progenitor masses) of the obscured C-stars in the SMC and LMC would be to obtain follow-up high-resolution ($R = \frac{\lambda}{\delta\lambda} > 20\,000$) near-IR (*JHK* bands) spectroscopy of these stars. This can be done with actual instrumentation (e.g. CRIRES at European Southern Observatory/VLT). From such spectra, one could get the CNO elemental abundances, which are expected to be different in both types of stars (see e.g. Ventura et al. 2015b).

On the other hand, an analysis of the chemical composition of planetary nebulae (PNe) in the MCs would provide important complementary information on the chemical enrichment of C-stars in these galaxies. This is because only small surface abundance changes are expected from the final AGB phase to the PN stage. For example, Ventura et al. (2015b) showed that the most C-enriched PNe in the LMC display carbon abundances below X(C) ∼ 0.01, in agreement with the 2.5 and 3 $M_\odot$ ATON models and with the 2.25 $M_\odot$ MONASH model (see the bottom-right panel in Fig. 1). The extension of this type of analysis to a much wider sample of PNe in the LMC (and also to the SMC PNe) will help us to understand whether this upper limit in the carbon abundance is real, or due to the limited sample of PNe examined.

7 CONCLUSIONS

We use *Spitzer* IR data of C-stars in the MCs to improve our understanding of the evolution of AGB stars with masses below ∼3 $M_\odot$, which become carbon stars through repeated TDU events. We focus on the objects with the highest degree of obscuration, because it is easier to characterize their progenitors in terms of their initial masses and metallicities. This is due to differences in the SFH between the SMC and the LMC, allowing us to investigate stars of different masses. The analysis of the SMC permits us to study the evolutionary properties of AGB stars of mass ∼1.5 $M_\odot$, whereas we use the LMC to investigate higher mass stars, with ∼2.5–3 $M_\odot$.

The LMC sequence of C-stars extends to redder IR colours ([3.6] − [4.5] ∼ 3) compared to the SMC ([3.6] − [4.5] ∼ 1.2). According to our interpretation, this is because of the higher quantity of carbonaceous dust forming in the circumstellar envelope of ∼2.5–3 $M_\odot$ stars, in comparison with their lower mass (∼1.5 $M_\odot$) counterparts evolving in the SMC.

The comparison between models and observations suggests the following: (a) in ∼1.5 $M_\odot$ AGB stars TDU must be efficient enough to produce a surface carbon abundance above X(C) ∼ 0.005 before the end of the AGB phase; (b) to correctly model the late AGB phases of stars of mass ∼2.5–3 $M_\odot$, it is mandatory to include the carbon enrichment in the calculation of the low-temperature molecular opacities (Marigo 2002; Ventura & Marigo 2009, 2010; Kamath et al. 2012). In addition, the description of mass-loss must rely on hydrodynamical simulations, which take into account dust formation. These physical ingredients are crucial in order to reproduce the extremely red colours of the C-stars in the LMC with the largest degree of obscuration. Based on our modelling, these stars evolve at effective temperatures close to ∼2000 K and lose their external mantle with a rate slightly above 10^{-4} $M_\odot$ yr^{-1}.

If our understanding is correct, we expect that the most obscured stars in the SMC are surrounded by a more internal region with SiC dust grains ∼0.06 μm sized, and a more external zone, ∼10 stellar radii from the surface of the star, where SiC grains and ∼0.2 μm sized, solid carbon particles are present. In the counterparts in the LMC, the higher metallicity favours a larger growth of SiC grains, which reach dimensions of the order of ∼0.06 μm. Solid carbon grains on the other hand can grow to ∼0.28 μm, because these stars are more enriched in gaseous carbon than their counterparts of smaller mass.

High-resolution near-IR spectroscopy of the most obscured C-stars in the SMC and LMC as well as the analysis of a wider MC PNe sample will allow us to test the conclusions reached here; i.e. the most obscured C-rich AGB stars in the LMC are the descendants of stars with higher initial masses than their SMC counterparts.

ACKNOWLEDGEMENTS

The authors are indebted to the referee, J. Th. van Loon, for the careful reading of the manuscript and for the several comments, which help improving significantly the quality of this work. PV was supported by PRIN MIUR 2011 'The Chemical and Dynamical Evolution of the Milky Way and Local Group Galaxies' (PI: F. Matteucci), prot. 2010LY5N2T. AIK was supported through an Australian Research Council Future Fellowship (FT110100475). DAGH was funded by the Ramón y Cajal fellowship number RYC−2013−14182 and he acknowledges support provided by the Spanish Ministry of Economy and Competitiveness (MINECO) under grant AYA−2014−58082-P. FD and MDC acknowledge support from the Observatory of Rome.

REFERENCES

Bessell M. S., Brett J. M., Wood P. R., Scholz M., 1989, A&AS, 77, 1
Blöcker T., 1995, A&A, 297, 727
Blum R. D. et al., 2006, AJ, 132, 2034
Boyer M. L. et al., 2011, AJ, 142, 103
Boyer M. L. et al., 2012, ApJ, 748, 40
Boyer M. L. et al., 2015, ApJ, 810, 116
Canuto V. M. C., Mazzitelli I., 1991, ApJ, 370, 295
Chiosi C., Wood P. R., Capitanio N., 1993, ApJS, 86, 541
Cioni M.-R. L. et al., 2000a, A&AS, 144, 235
Cioni M.-R. L., Habing H. J., Israel F. P., 2000b, A&A, 358, L9
Cioni M.-R. L., Girardi L., Marigo P., Habing H. J., 2006, A&A, 448, 77
Dell'Agli F., Ventura P., García-Hernández D. A., Schneider R., Di Criscienzo M., Brocato E., D'Antona F., Rossi C., 2014, MNRAS, 442, L38
Dell'Agli F., Ventura P., Schneider R., Di Criscienzo M., García-Hernández D. A., Rossi C., Brocato E., 2015a, MNRAS, 447, 2992
Dell'Agli F., García-Hernández D. A., Ventura P., Schneider R., Di Criscienzo M., Rossi C., 2015b, MNRAS, 454, 4235
Di Criscienzo M. et al., 2013, MNRAS, 433, 313
Epchtein N. et al., 1994, Ap&SS, 217, 3
Ferrarotti A. D., Gail H. P., 2001, A&A, 371, 133
Ferrarotti A. D., Gail H. P., 2002, A&A, 382, 256
Ferrarotti A. D., Gail H. P., 2006, A&A, 553, 576
Frost C. A., Lattanzio J. C., 1996, ApJ, 473, 383

Downloaded from http://mnras.oxfordjournals.org/ at NASA Goddard Space Flight Ctr on May 24, 2016

Gail H. P., Sedlmayr E., 1985, A&A, 148, 183
Gail H. P., Sedlmayr E., 1999, A&A, 347, 594
Gordon K. D. et al., 2011, AJ, 142, 102
Groenewegen M. A. T., de Jong T., 1993, A&A, 267, 410
Groenewegen M. A. T. et al., 2007, MNRAS, 376, 313
Gullieuszik M. et al., 2012, A&A, 537, A105
Harris J., Zaritsky D., 2004, AJ, 127, 1531
Harris J., Zaritsky D., 2009, ApJ, 138, 1243
Izzard R. G., Tout C. A., Karakas A. I., Pols O. R., 2004, MNRAS, 350, 407
Kamath D., Karakas A. I., Wood P. R., 2012, ApJ, 746, 20
Karakas A. I., 2010, MNRAS, 403, 1413
Karakas A. I., Lattanzio J. C., 2014, PASA, 31, e030
Karakas A. I., Lattanzio J. C., Pols O. R., 2002, PASA, 19, 515
Karakas A. I., Campbell S. W., Stancliffe R. J., 2010, ApJ, 713, 374
Keller S. C., Wood P. R., 2006, ApJ, 642, 834
Lagadec E. et al., 2007, MNRAS, 376, 1270
Lattanzio J. C., 1986, ApJ, 311, 708
Maiolino R., Schneider R., Oliva E., Bianchi S., Ferrara A., Mannucci F., Pedani M., Roca Sogorb M., 2004, Nature, 431, 533
Maraston C., Daddi E., Renzini A., Cimatti A., Dickinson M., Papovich C., Pasquali A., Pirzkal N., 2006, ApJ, 652, 85
Marigo P., 2002, A&A, 387, 507
Marigo P., Aringer B., 2009, A&A, 508, 1538
Marigo P., Girardi L., 2007, A&A, 469, 23
Marigo P., Girardi L., Bressan A., 1999, A&A, 344, 123
Marigo P., Girardi L., Bressan A., Groenewegen M. A. T., Silva L., Granato G. L., 2008, A&A, 482, 883
Meixner M. et al., 2006, AJ, 132, 2268
Meixner M. et al., 2010, A&A, 518, L71
Meixner M. et al., 2013, ApJ, 146, 62
Nanni A., Bressan A., Marigo P., Girardi L., 2013a, MNRAS, 434, 488
Nanni A., Bressan A., Marigo P., Girardi L., 2013b, MNRAS, 434, 2390
Nanni A., Bressan A., Marigo P., Girardi L., 2014, MNRAS, 438, 2328
Nozawa T., Kozasa T., Umeda H., Maeda K., Nomoto K., 2003, ApJ, 598, 785
Riebel D., Srinivasan S., Sargent B., Meixner M., 2012, AJ, 753, 71
Romano D., Karakas A. I., Tosi M., Matteucci F., 2010, A&A, 522, A32
Santini P. et al., 2014, A&A, 526, A30
Skrutskie M. F. et al., 2006, AJ, 131, 1163
Sloan G. C., Kraemer K. E., Wood P. R., Zijlstra A. A., Bernard-Salas J., Devost D., Houck J. R., 2008, ApJ, 686, 1056
Srinivasan S. et al., 2009, AJ, 137, 4810
Srinivasan S., Sargent B. A., Meixner M., 2011, A&A, 532, A54
Stancliffe R. J., Izzard R. G., Tout C. A., 2005, MNRAS, 356, L1
Todini P., Ferrara A., 2001, MNRAS, 325, 726
Valiante R., Schneider R., Salvadori S., Bianchi S., 2011, MNRAS, 416, 1916
van Loon J., 2006, in Armus L., Reach W. T., eds, ASP Conf. Ser. Vol. 357, The Spitzer Space Telescope: New Views of the Cosmos. Astron. Soc. Pac., San Francisco, p. 155
van Loon J. Th., Zijlstra A. A., Groenewegen M. A. T., 1999, A&A, 346, 805
van Loon J. Th., Marshall J. R., Cohen M., Matsuura M., Wood P. R., Yamamura I., Zijlstra A. A., 2006, A&A, 447, 971
van Loon J. T., Cohen M., Oliveira J. M., Matsuura M., McDonald I., Sloan G. C., Wood P. R., Zijlstra A. A., 2008, A&A, 487, 1055
Vassiliadis E., Wood P. R., 1993, ApJ, 413, 641
Ventura P., D'Antona F., 2005, A&A, 431, 279
Ventura P., Marigo P., 2009, MNRAS, 399, L54
Ventura P., Marigo P., 2010, MNRAS, 408, 2476
Ventura P., Zeppieri A., Mazzitelli I., D'Antona F., 1998, A&A, 334, 953
Ventura P., D'Antona F., Mazzitelli I., Gratton R., 2001, ApJ, 550, L65
Ventura P. et al., 2012a, MNRAS, 420, 1442
Ventura P. et al., 2012b, MNRAS, 424, 2345
Ventura P., Di Criscienzo M., Carini R., D'Antona F., 2013, MNRAS, 431, 3642
Ventura P., Dell'Agli F., Di Criscienzo M., Schneider R., Rossi C., La Franca F., Gallerani S., Valiante R., 2014, MNRAS, 439, 977
Ventura P., Karakas A. I., Dell'Agli F., Boyer M. L., García-Hernández D. A., Di Criscienzo M., Schneider R., 2015a, MNRAS, 450, 3181
Ventura P., Stanghellini L., Dell'Agli F., García-Hernández D. A., Di Criscienzo M., 2015b, MNRAS, 452, 3679
Wachter A., Schröder K. P., Winters J. M., Arndt T. U., Sedlmayr E., 2002, A&A, 384, 452
Wachter A., Winters J. M., Schröder K. P., Sedlmayr E., 2008, A&A, 486, 497
Westerlund B. E., 1997, The Magellanic Clouds. Cambridge Univ. Press, Cambridge
Yang X., Chen P., He J., 2004, A&A, 414, 1049
Zaritsky D., Harris J., Thompson I. B., Grebel E. K., 2004, AJ, 128, 1606
Zhukovska S., Gail H.-P., Trieloff M., 2008, A&A, 479, 453
Zijlstra A. A. et al., 2006, MNRAS, 370, 1961

This paper has been typeset from a TEX/LATEX file prepared by the author.

Downloaded from http://mnras.oxfordjournals.org/ at NASA Goddard Space Flight Ctr on May 24, 2016